33RD CONGRESS
OF THE INTERNATIONAL COUNCIL
OF THE AERONAUTICAL SCIENCES
STOCKHOLM, SWEDEN, 4-9 SEPTEMBER, 2022

ICAS 2022 SWEDEN

OPEN CAVITY SIMULATIONS UNDER SIDESLIP FLOW CONDITIONS

Karthick Rajkumar[1], Joseph Radtke[1], Eike Tangermann[1] & Markus Klein[1]

[1]University of the Bundeswehr Munich, Werner-Heisenberg-Weg 39, 85577 Neubiberg, Germany

Abstract

Resonant modes can be a hindrance to store release in weapon bays of fighter aircraft, which feature a typical open cavity configuration. Transonic flow over such an open cavity with a length to depth ratio of 5.7 has been investigated numerically under the angle of attack (α) 0° and angle of sideslip (β) 8° to understand the directional impact of flow processes on the Rossiter modes and their modulations. Employing the turbulence-resolving approach of scale-adaptive simulation (SAS), various flow aspects of the cavity configuration have been investigated and will be discussed in this article along with the validation of the numerical results. Furthermore, the mechanisms by which the resonant modes are affected are presented with the help of spectral analysis.

Keywords: Rossiter modes, Scale-adaptive simulation, open cavity flows

1. Introduction

In aeronautical applications, interior storage carriages, such as weapon bays feature a typical open cavity configuration, wherein a complex, unsteady interaction between aerodynamic instabilities and acoustic waves occurs. It has the tendency to exhibit resonance and produce dominant modes inside the cavity, which can lead to structural fatigue and impede store release. In order to mitigate the effects of resonance in the weapon bay design process, it is necessary that the flow mechanism is understood and appropriate design changes are considered.

A typical acoustic spectrum of an open cavity flow consists of broadband noise and narrow-band tones. The high amplitude tones developed inside the cavity are called Rossiter modes, named after Rossiter [1], who postulated a semi-empirical model to estimate the frequencies at which the modes occur. Rossiter described the mechanism of distinct modes appearing in the open cavity. He devised the oscillation model (equation 1) based on three observations inside the cavity: 1. downstream convection of vortices from the shear layer, 2. impingement of vortices at the downstream edge generating acoustic waves and 3. acoustic waves travelling upstream and exciting further disturbances in the shear layer, leading to a self-sustained oscillation process.

$$f = \frac{U_\infty}{L}\frac{m-\alpha}{Ma+1/\kappa} \tag{1}$$

Here f is the frequency at which the modes appear, U_∞ is the freestream velocity, L is the length of the cavity, m is the mode number, α is the phase delay constant, Ma is the Mach number and κ is the ratio of convection velocity of vortical structure to the freestream velocity.

Much of the cavity flow research has been experimental. The study by Rossiter [1] was one of the foremost studies that provided a solid understanding of the physics-based acoustic-flow dynamic interaction. The model by Rossiter (equation 1) is still widely used to predict the modes, particularly in the subsonic and transonic flow conditions. However, the model has shown some inaccuracies in supersonic flow conditions. Heller et al. [2] modified the Rossiter model by assuming that the speed of sound inside the cavity is equal to that in the stagnating freestream and the resulting modified Rossiter model holds its validity in supersonic conditions as well. Handa et al. [3] have studied the

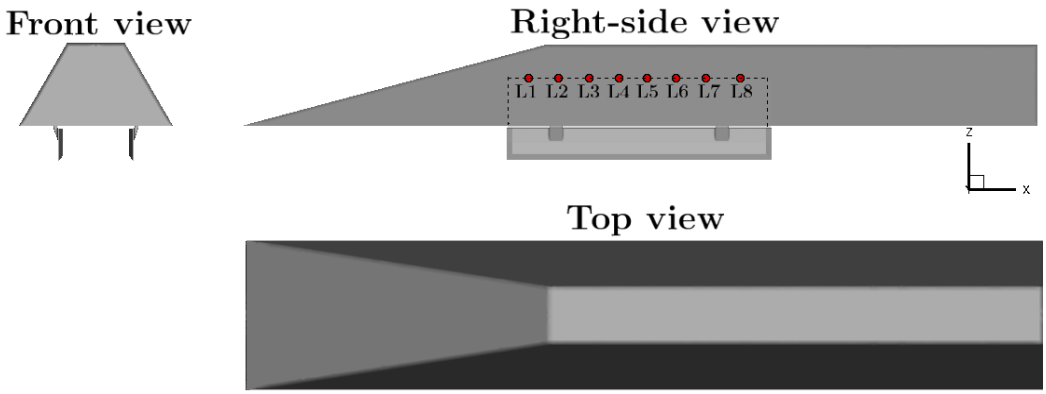

Figure 1 – Model of the open cavity with side doors

generation and propagation of pressure waves in the cavity experimentally for supersonic flow past a deep rectangular cavity. The study explains the process by which the pressure waves are generated and the path of the pressure waves was investigated. It tries to clarify the relationship between the shear-layer motion, pressure-wave generation and the pressure oscillation inside the cavity.
In literature, a number of open cavity flow studies exist with symmetric flow conditions ($\beta = 0°$) and the resonant process has been shown to be predominantly 2D in nature. To the author's knowledge, there is hardly any study featuring asymmetric transonic flow conditions. In previous studies [4] and [5], the open cavity configuration presented in the work by Mayer et. al. [6] has been studied numerically using the DLR-TAU code [7] for transonic and symmetric flow conditions. The work also includes the investigations into methodologies of turbulence treatment, namely the scale-adaptive simulation (SAS) towards reducing the computational cost of simulating cavity flows while maintaining good accuracy relative to hybrid RANS-LES results and experimental data. In this work, the configuration is further extended to include non-zero sideslip flow conditions to understand the directional impact of flow processes on the Rossiter modes and their modulations. Under this scope, a flow with the conditions of Mach number (Ma) 0.8 and Reynolds number (Re) 8×10^6 with $\beta = 8°$ has been simulated using the scale-adaptive simulation. Flow investigations are presented and the spectral results explaining the presence of Rossiter modes and their modulations under sideslip flow conditions are outlined.

2. Geometry and mesh

The cavity configuration used in this study is shown in Fig. 1. A cuboid cavity with length to depth ratio (L/D) 5.7 and length to width ratio (L/W) 4.16 is cut into a flat side of a test rig at a certain distance from its sharp leading edge and on the centre line. The doors are placed on either side of the cavity with positive Z pointing into the cavity. The probe locations placed at equidistant locations along the cavity ceiling and named L1 to L8.
The cavity geometry has been spatially discretized with a mesh consisting of unstructured elements with tetrahedral, prism, hexahedral and pyramid cells (Fig. 2). The model was initially simulated with the RANS k-ω model to estimate integral length scales of the flow features. Based on the estimates, approximately $1-2$ cells have been placed in and around the cavity and have been meshed. The resulting mesh was computed with the scale-resolving SAS model. It has been ensured that the universal $-5/3$ power law [8] is satisfied for a few probe locations in the shear layer. From experience, it is understood that there are a few physical factors to be considered during the meshing stage. The boundary layer resolution upstream of the wall is crucial, as it leads to the formation of the shear layer after it separates. The shedding of vortices in the shear layer is one of the major contributors to the sustained oscillation process, therefore a particular attention has been given to resolve the shear layer region where the vortices are generated. The disturbances from the vortices propagate and resonate with the upstream travelling waves that are reflected from the rear wall where the flow impingement occurs. Therefore, sufficient mesh density has to be maintained at the impingement location on the rear wall. Furthermore, the model has been meshed in half and mirrored about the

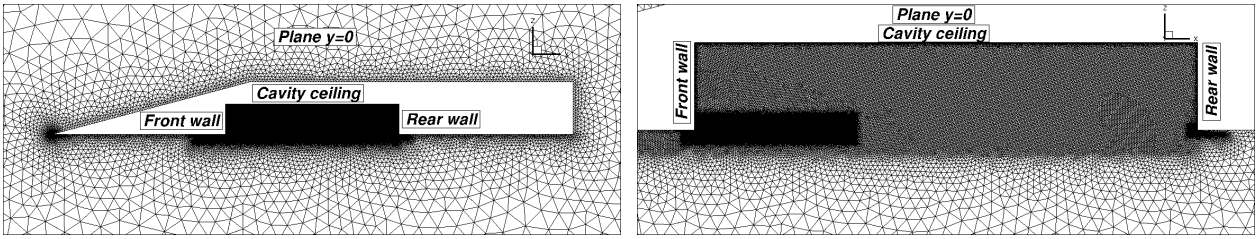

(a) Mesh distribution at slice plane y=0 (b) Closer view inside the cavity

Figure 2 – Computational mesh

symmetry axis so that asymmetric grid effects are effectively avoided. The mesh is composed of 5×10^6 elements. Moreover, the non-dimensional thickness (y^+) of the first cell layer has been set to be less than unity.

3. Numerical approach

Compressible Navier-Stokes equations employing the Finite Volume Method (FVM) have been solved in this study using the CFD DLR-TAU code [7]. The concept of turbulence modelling employed is based on the work by Menter et al. [9], which suggested a modified turbulence model that adds a source term Q_{SAS} based on the local von Karman length scale L_{vK} to only resolve major turbulent scales. This scale-resolving technique has been used in this study with the standard $k-\omega$ SST model [10] as the base model. The governing equations of the SST-SAS model differ from the $k-\omega$ SST model by the additional source term Q_{SAS} in the transport equation for the turbulence eddy frequency ω which is defined as shown in Eq. 2. This approach has been shown to simulate the cavity flows efficiently capturing the essential cavity flow physics in the author's previous studies for the symmetric flow conditions ([4], [5]).

$$Q_{SAS} = max\left[\rho\zeta_2 S^2\left(\frac{L}{L_{vK}}\right)^2 - F_{SAS}\frac{2\rho k}{\sigma_\phi} max\left(\frac{1}{k^2}\frac{\partial k}{\partial x_j}\frac{\partial k}{\partial x_j}, \frac{1}{\omega^2}\frac{\partial \omega}{\partial x_j}\frac{\partial \omega}{\partial x_j}\right), 0\right] \tag{2}$$

The von Karman length scale L_{vK} is given by

$$L_{vK} = \kappa\frac{U'}{U''}; \quad U'' = \sqrt{\frac{\partial^2 u_i}{\partial x_k^2}\frac{\partial^2 u_i}{\partial x_j^2}}; \quad U' = \sqrt{2\cdot S_{ij}S_{ij}}$$

with $k = 0.41$, $\zeta_2 = 1.755$, $\sigma_\phi = 2/3$ and $F_{SAS} = 1.25$.

The SAS model can be considered as a scale-resolving URANS model, which can show LES-like behavior. Unlike LES, it also remains well-defined if the mesh cells get coarser and do not allow resolving scales well within the inertial range. This makes it attractive in the present application, where the aero-acoustic effects are mostly affected by larger turbulent scales which, in turn, need to be predicted accurately.

A second-order central scheme and backward Euler scheme have been used to discretize spatial flux and temporal terms, respectively. The time step size has been chosen such that the convective Courant-Friedrichs-Lewy number (CFL) is below 1.0.

4. Results and discussion

In this section, some of the flow investigations of the cavity along with validation of numerical results will be discussed.

4.1 Instantaneous flow field

As observed in the previous studies with $\beta = 0^\circ$ [4] and [5], where the shear layer is formed from the front edge of the cavity, it is observed for the $\beta = 8^\circ$ case as well that the shear layer separates from the front edge of the cavity. However, there are more structures added to the shear layer from the edge of the windward-side door (marked in circle in Fig. 3). At the intersection of the windward door and the front edge of the cavity, the shedding flow structures merge and travel downstream.

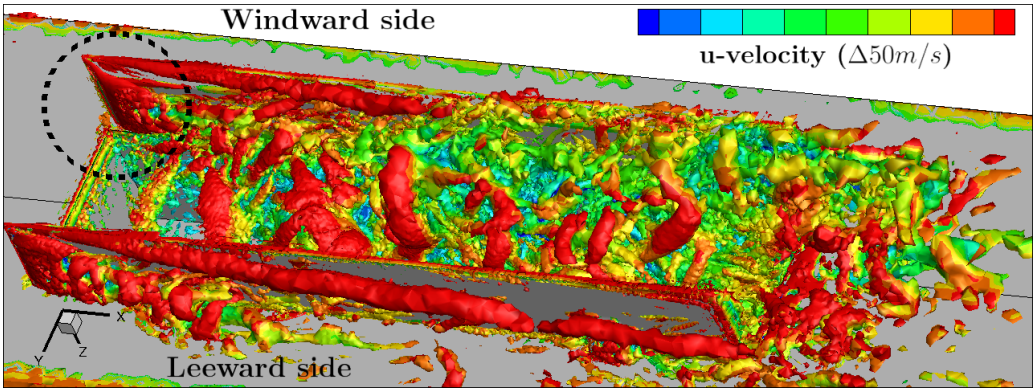

Figure 3 – Evolution of flow structures observed through Q-criterion

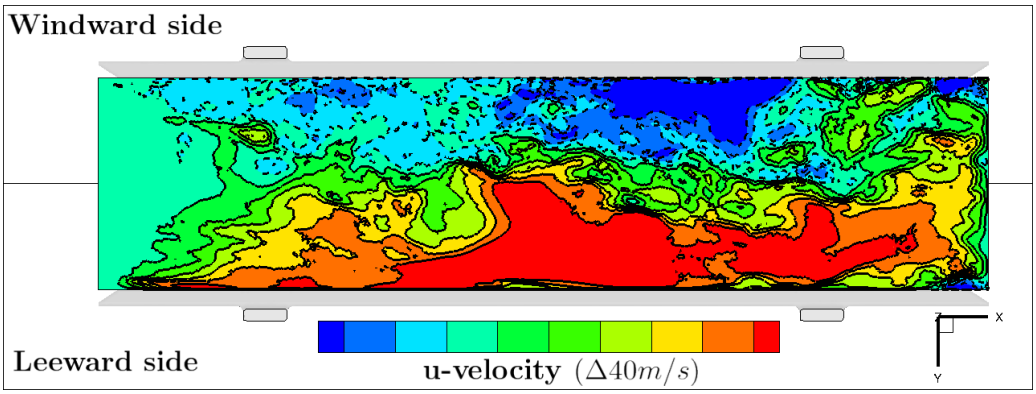

Figure 4 – Instantaneous streamwise velocity at plane $Z = 0.1D$

After merging, they grow in size while being convected in the shear layer before impinging on the end of the leeward-side door and on the rearwall of the cavity. On impingement, the flow redirects spanwise towards the bottom of the cavity, flows upstream and interacts with the oncoming shear layer. This spanwise recirculation process is identified as a typical characteristic of the cavity flow under asymmetric flow conditions (see Fig. 4). The spanwise recirculation can be seen with the negative u-velocity marked with a dotted line in Fig. 4. Such a spanwise recirculation process does not exist in symmetric flow conditions which is dominated by a streamwise recirculation. The turbulence resolving capability as seen in Fig. 3 is attributed to the usage of the underlying SAS model, which resolves turbulence when local fluctuations are present. The activation of the model is presented in Fig. 5 which shows the distribution of the local von Karman length scale L_{vK} at the same instant in time as in Fig. 4. On these regions where the value is higher, the turbulence scale is resolved to the underlying cell size and subsequently, eddy viscosity is reduced at these locations. The scales are seen concentrated in the middle region where high fluctuations are present.

4.2 Unsteady characteristics

Fig. 6 shows the experimental results by depicting the modulation effect of the sideslip angles on the spectral modes. It is evident that as the sideslip angle increases, the frequencies at which the resonant modes occur reduce and the modal amplitudes increase. It has been reported in the study [4] that using wall functions leads to stronger vortices in the shear layer and subsequent overprediction of spectral amplitudes, although the spectral frequencies are intact and in agreement with the experimental data. This confirms that, in principle, the Rossiter frequencies are correlated to the interaction time scale between the aerodynamic disturbances from the shear layer and upstream travelling acoustic waves. This interaction time scale is a direct consequence of the length of the cavity, as seen also in the Rossiter model for frequency estimation (equation 1). As the sideslip angle increases, the interaction time scale between them increases due to the skewed shear layer flow inside the cavity and peak frequencies decrease as a result. The Rossiter magnitudes are correlated to the interference of various pressure waves reflected from all walls of the cavity, shear layer distur-

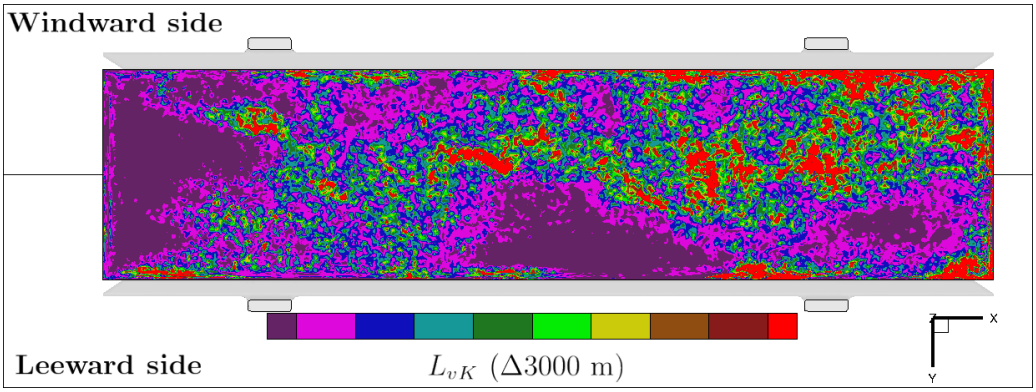

Figure 5 – von Karman length scale at plane $Z = 0.1D$

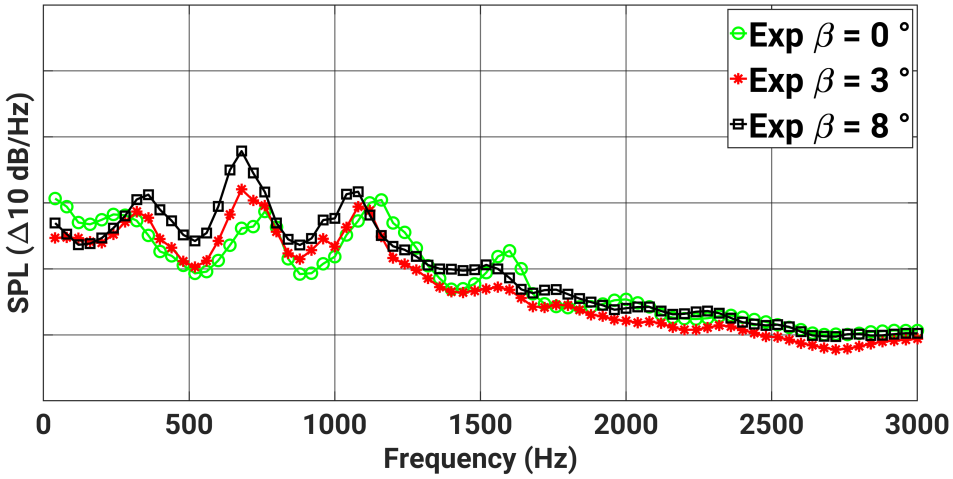

Figure 6 – Effect of sideslip angle on the Rossiter modes

bances and impingement-induced waves. The increase in the spectral magnitudes with increasing sideslip angles could be due to a more signifcant contribution from the spanwise travelling waves to the spectral modes. It is to be noted that the shear layer in the asymmetric flow conditions exhibits a vast range of flow scales in the spanwise direction due to the contribution of flow structures from the door, as opposed to similar spanwise flow scales in the symmetric flow conditions. This could in essence contribute to waves propagating and reflecting in a more complex manner comprising a range of amplitudes and wavelengths within the walls of the 3D cavity.

In the $\beta = 8^{\circ}$ case, it is suspected that the region encompassing the cavity sidewall on the leeward side along with the rearwall of the cavity reflects the pressure waves due to intense pressure fluctuations in these regions as seen in Fig. 7. The pressure fluctuations are seen intense not only on the rear wall but also on the leeward-side door. The pressure waves reflect from the side door travel in the spanwise direction and would then lead to superposition and eventual modulation of the spectral modes.

In order to understand the flow physics in detail, the pressure data have been collected for a few thousand locations encompassing the cavity and a Fast Fourier Transform (FFT) has been performed based on Welch's method and to decompose the fluctuations into their frequency components. Fig. 8 shows FFT spectrum of the probe locations along the cavity ceiling, where the measurement data is available. It is obvious that the shape of the Rossiter modes occurring in all the probe locations has been predicted in good agreement with the experimental data. In addition to the shape of the modes, also the relative magnitudes between the modes have been predicted well. The dominant mode 2 has been marginally under-predicted by the simulation for all the probe locations.

The amplitude of the first four resonance modes was identified and visualized on different planes to indentify the shape of the modes and to aid in deeper understanding of the flow physics. The results can be seen in Fig. 9 showing the Sound Pressure Level (SPL) distribution of the Rossiter

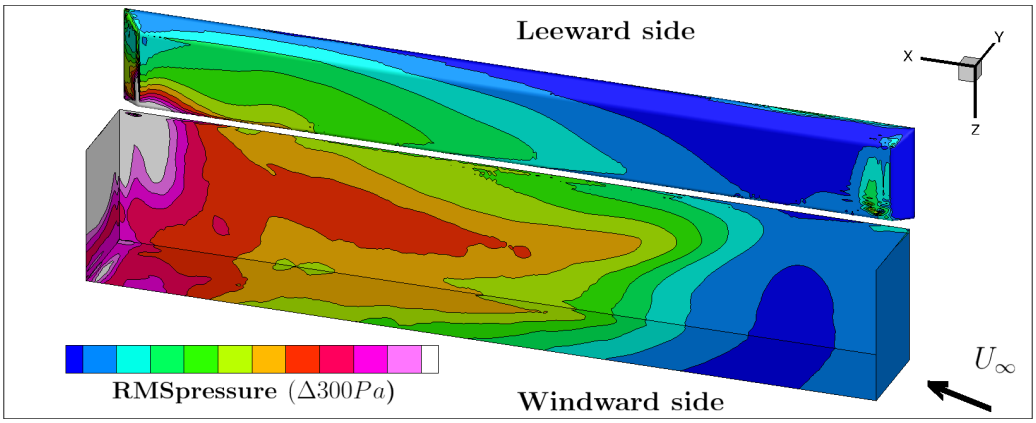

Figure 7 – RMS pressure distribution

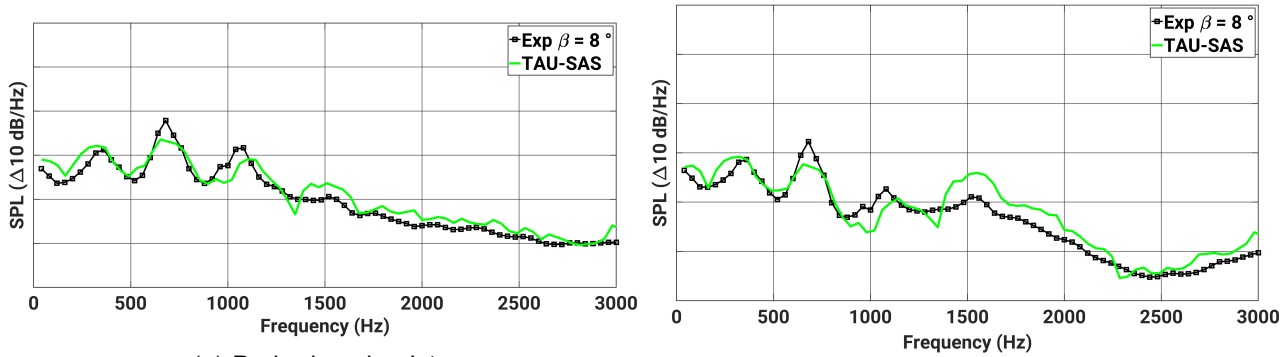

(a) Probe location L1

(b) Probe location L2

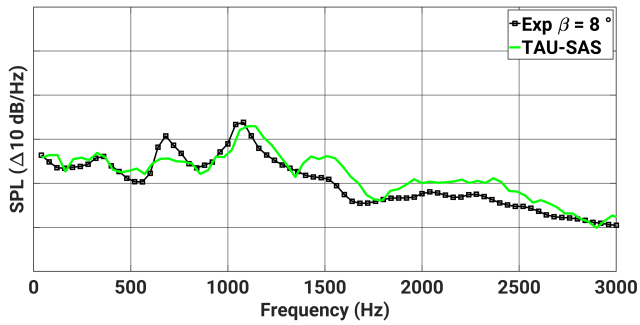

(c) Probe location L3

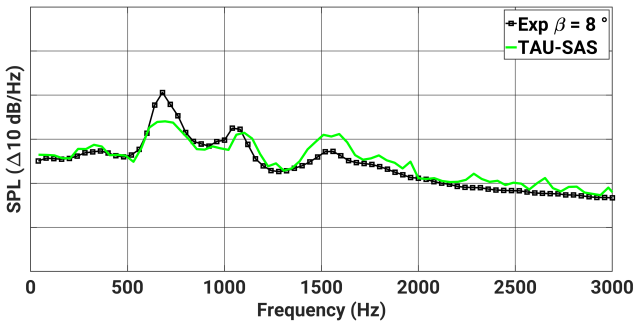

(d) Probe location L4

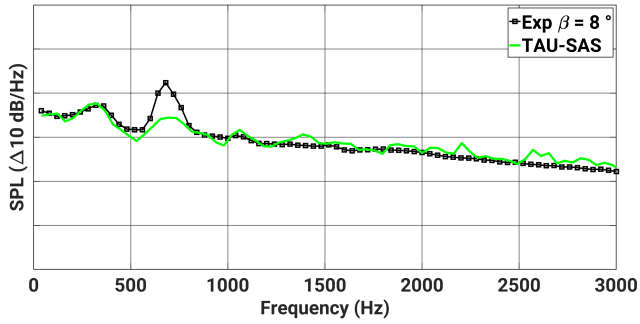

(e) Probe location L7

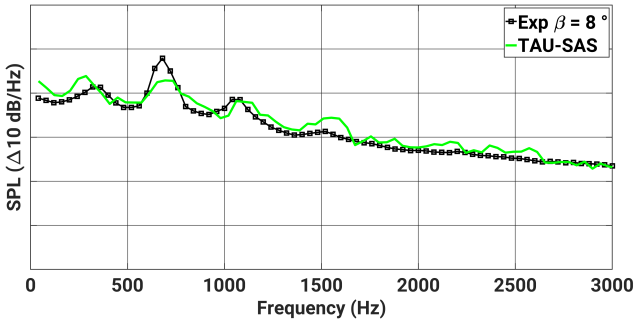

(f) Probe location L8

Figure 8 – SPL of probe locations

modes 1 to 4 on different spanwise planes, with plane $Z = 0.95D$ being closest to the ceiling. From an overview of all the plots, it is obvious that there is a longitudinal or streamwise propagation of waves with wavelength of modes becoming smaller with increase in the mode number. In addition to the longitudinal waves, one can also visualize the contribritution of spanwise propagating waves.
Mode 1 is governed by the bulk flow processes in the cavity, namely the shear layer and the spanwise recirculation process. The shear layer in the upper half of the cavity (Fig. 9a and 9b) gives rise to mode 1 with its anti-node present at the interaction of the shear layer with the upstream flow. At the lower half of the cavity (Fig. 9c and 9d), the recirculation process dominates the mode 1 oscillation. The resonance between these two large scale mechanisms, in principle, sustains and feeds mode 1 in the cavity.
Scales that are smaller than the mode 1 in the shear layer feed mode 2, which in Fig. 9a shows the scales that come in contact with the leeward-side wall with the presence of an anti-node. Following the anti-node through all the spanwise planes in Fig. 9, it is apparent that the mode 2 is a 3D wave and has a contribution from spanwise travelling waves. This contribution results in the increase of modal amplitudes for asymmetric flow conditions.
Similarly, modes 3 and 4 have further smaller scales originating from the shear layer that come in contact with the leeward-side wall further upstream than its predecessor. One can see many spanwise travelling contributing waves in addition to the streamwise travelling waves. Furthermore, in the streamwise direction, more nodes with shorter wavelengths exist with increasing mode number. Overall, it can be seen that the flow structures in the shear layer drive the flow oscillations. At the asymmetric flow condition, in addition to the streamwise travelling waves, a significant wave interference takes place in the spanwise direction.

5. Conclusion

In this study, an open cavity flow with the conditions of Mach number (Ma) 0.8 and Reynolds number (Re) 8×10^6 with the sideslip angle $\beta = 8^\circ$ has been simulated using the SAS turbulence model. The instantaneous flow fields and the unsteady characteristics have been presented and discussed along with the spectral results. The validation of the numerical results has been presented using the experimental data collected for probe locations along the cavity ceiling. Furthermore, the mechanism behind the Rossiter modes under sideslip conditions and their modulations has been discussed. It has been shown that a complex interference of waves occurs in a highly three-dimensional manner between the walls of the cavity.

6. Acknowledgements

This work has been carried out with the financial support from Airbus Defence and Space (ADS) under the project "Analysis of Unsteady Effects in Fighter Aircraft Aerodynamics", which is greatly acknowledged. Furthermore, the experimental survey has been carried out by ADS and made available to this study for the validation of numerical results. The authors would like to thank the German Aerospace Center (DLR) for providing the TAU CFD code and Ennova Technologies, Inc. for the meshing software. The authors would also like to acknowledge the Gauss Centre for Supercomputing for making the required computing hours available to this study.

7. Contact Author Email Address

mailto: karthick.rajkumar@unibw.de

8. Copyright Statement

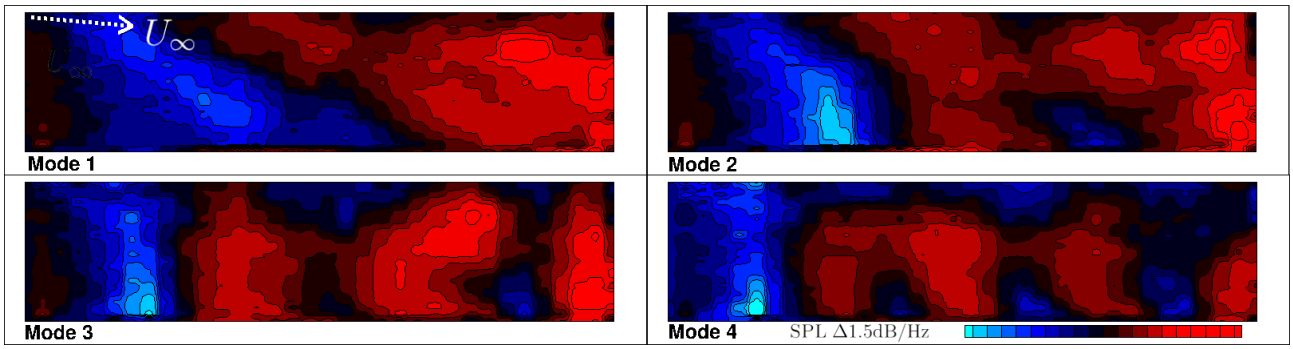

(a) SPL distribution at plane $Z = 0.1D$

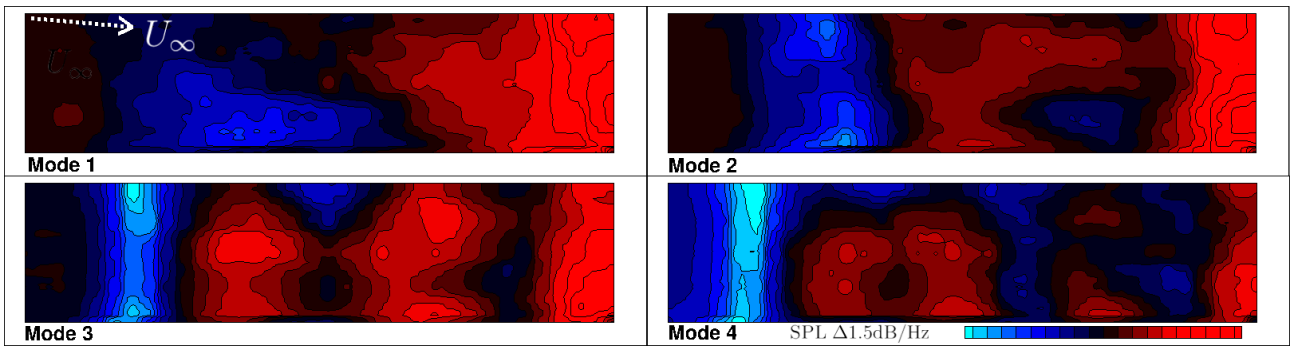

(b) SPL distribution at plane $Z = 0.25D$

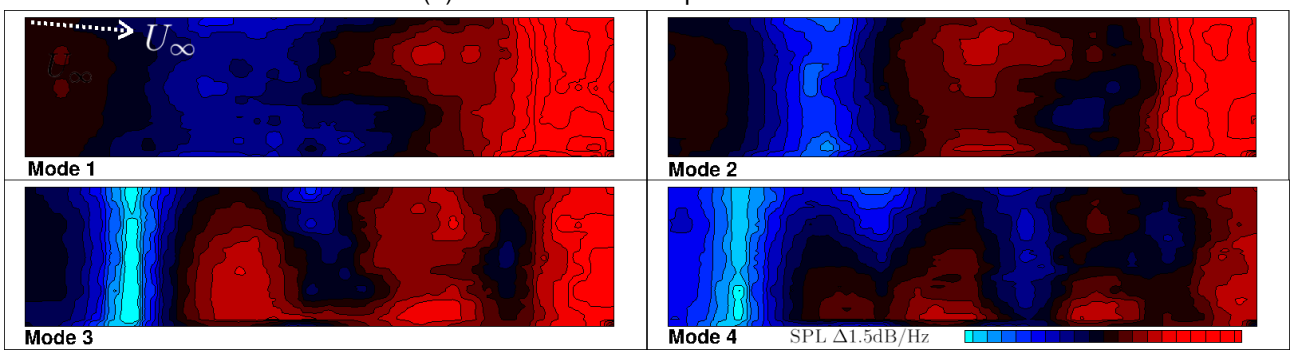

(c) SPL distribution at plane $Z = 0.75D$

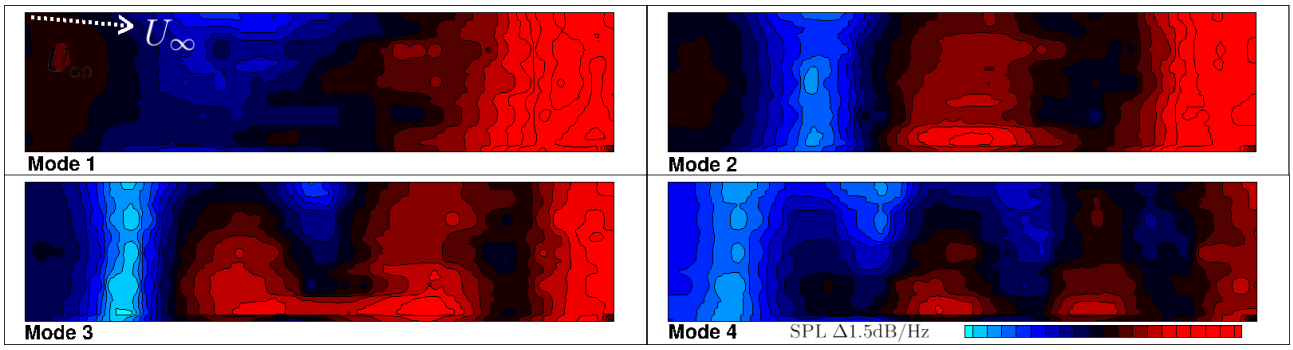

(d) SPL distribution at plane $Z = 0.95D$

Figure 9 – SPL distribution at different Z planes

References

[1] J.E. Rossiter. Wind tunnel experiments on the flow over rectangular cavities at subsonic and transonic speeds, 1964.

[2] H. H. Heller, D. G. Holmes, and E. E. Covert. Flow-induced pressure oscillations in shallow cavities. *Journal of Sound and Vibration*, 18:545–553, 1971.

[3] T. Handa, H. Miyachi, H. Kakuno, T. Ozaki, and S. Maruyama. Modeling of a feedback mechanism in supersonic deep-cavity Flows. *AIAA Journal*, 53(2):420–425, oct 2015.

[4] K. Rajkumar, E. Tangermann, M. Klein, S. Ketterl, and A. Winkler. Time-efficient simulations of weapon bay in fighter aircraft. *Aerospace Europe Conference, Poland*, 2021.

[5] K. Rajkumar, E. Tangermann, M. Klein, S. Ketterl, and A. Winkler. DES of weapon bay in fighter aircraft under high-subsonic and supersonic conditions. *Notes on Numerical Fluid Mechanics and Multidisciplinary Design*, 151:656–665, 2021.

[6] F. Mayer, S. Mancini, and A. Kolb. Experimental investigation of installation effects on the aeroacoustic behaviour of rectangular cavities at high subsonic and supersonic speed. *Deutscher Luft- und Raumfahrtkongress, Germany*, 2020.

[7] S. Langer, A. Schwöppe, and N. Kroll. The DLR flow solver TAU - status and recent algorithmic developments. *52nd Aerospace Sciences Meeting*, 2014.

[8] A.N Kolmogorov. The Local Structure of Turbulence in Incompressible Viscous Fluid for Very Large Reynolds Numbers. *Doklady Akademii Nauk SSSR*, 30:301–304, 1941.

[9] F. R. Menter, A. Garbaruk, P. Smirnov, D. Cokljat, and F. Mathey. Scale-adaptive simulation with artificial forcing. *Notes on Numerical Fluid Mechanics and Multidisciplinary Design*, 111(January):235–246, 2010.

[10] F. R. Menter. Two-equation eddy-viscosity turbulence models for engineering applications. *AIAA Journal*, 32(8):1598–1605, 1994.